ISSN No:-2456-2165

Lung Lesion Localization of COVID-19FromChest CT Image using Behavioral Mapping and Tracking

Ms. CH. SRILAKSHMI[1], Gowtham H[2], Jashvanth S R[3]
[1]Associate Professor, Computer Science and Business Systems, R.M.D.Engineering College
[2]UG Scholar, Computer Science and Business Systems, R.M.D.Engineering College
[3]UG Scholar, Computer Science and Business Systems, R.M.D.Engineering College

Abstract:- Coronavirus Disease 2019 requires chest computed tomography (CT) imaging data for early diagnosis, treatment, and prognosis (COVID-19). Artificial intelligence has been triedto assist physicians in enhancing the diagnosisaccuracy and operating efficiency of CT. Existing supervised techniques on CT images of COVID- 19 pneumonia require voxel-based annotations for training, which takes a long time and effort. This research developed a weakly-supervised technique for COVID-19 lesion localization based on generative adversarial networks (GAN) using just image-level labels. We originally presented a GAN-based framework for generating normal- looking CT slices from CT scans with COVID-19 lesions. We then devised a unique feature matching technique to enhance the realism of produced pictures by directing the generator tocapture the intricate texture of chest CT images. Finally, by subtracting the output picture from its matching input image, the localization map of lesions may be simply generated. We can increasethe classification accuracy of our diagnostic system by adding a classifier branch to the GAN- based architecture to identify localization maps.In this paper, three CT datasets regarding COVID-19 were obtained for examination from hospitals in Sao Paulo, the Italian Society of Medical and Interventional Radiology, and China Medical University. Our method of weakly supervised learning yielded AUC of 0.883, dice coefficient of 0.575, accuracy of 0.884, sensitivityof 0.647, specificity of 0.929, and F1-score of0.640 significantly outperformed other frequently used weakly supervised object localization algorithms. In addition, we compared the suggested technique to fully supervised learning methods in the COVID-19 lesion segmentationproblem, and the proposed weakly supervised method still produces a competitive performance with a dice coefficient of 0.575. Furthermore, we examined the relationship between illness severityand visual score and discovered that the common severity cohort had the largest sample size as well as the highest visual score, implying that our method can aid in the rapid diagnosis of COVID- 19 patients, particularly in the massive common severity cohort .Finally, we argued that this uniquetechnique may be used as an accurate andefficient tool to remove the bottleneck of expert annotation costs and promote the advancement of computer-aided COVID-19 diagnosis.

Keywords:- *Coronavirus Disease 2019, Generative Adversarial Network, Lesion Location, and Lesion Segmentation.*

I. INTRODUCTION

The global spread of the Coronavirus Disease 2019 (COVID-19) pandemic, caused by the severe acute respiratory syndrome coronavirus 2 (SARS-CoV-2), has posed a significant risk toglobal public health security. At the moment, early quick identification and management for this recently identified virus are in their infancy. Although reverse transcription polymerase chain reaction (RT-PCR) is commonly employed for COVID-19 screening, it has been demonstrated to have a significant false-negative rate. Because it has a faster testing cycle and can offer more precise information about the pathology as well as help evaluate the degree or severity of lung involvement, chest computed tomography (CT) has been highlighted as an essential complementary technique for the diagnosis of COVID-19. Manually defining the affected lung area, on the other hand The diagnosis of COVID- 19 based on chest CT imaging by radiologists is a time-consuming and subjective job. Artificial intelligence (AI) is fast being developed to operate in conjunction with CT to assist radiologists and doctors in improving diagnosis accuracy and working efficiency. Convolutional neural networks (CNNs) have become moreversatile as a result of effective regularisation algorithms and fast graphics processing units, allowing CNN structures to develop in depth and complexity, width, significantly improving learning capacity CNN-based computer-aided diagnosis (CADs) of COVID-19 have been extensively researched and may be split into two groups.

The automated COVID-19 diagnosis based on CT volumes or slices is the most popular. Forexample, Bai et al. propose an Efficient Net-based model for CT slice classification and claim that deep learning assisted radiologists in identifying COVID-19 from non-COVID-19 at chest CT. Wang et al., on the other hand, aim to use a 3D CNN with a 3D lung mask to make decisions directly. However, the CNN-based categorization model can only deliver final conclusions and lacks reasoning capability. Despite the fact that visualisation techniques such as Gradient- weighted Class Activation Mapping (Grad-CAM)can be employed to alleviate this scarcity, the lesion localization map created by such visualization approaches coarse and provides less valuable information for treatment evaluation.

ISSN No:-2456-2165

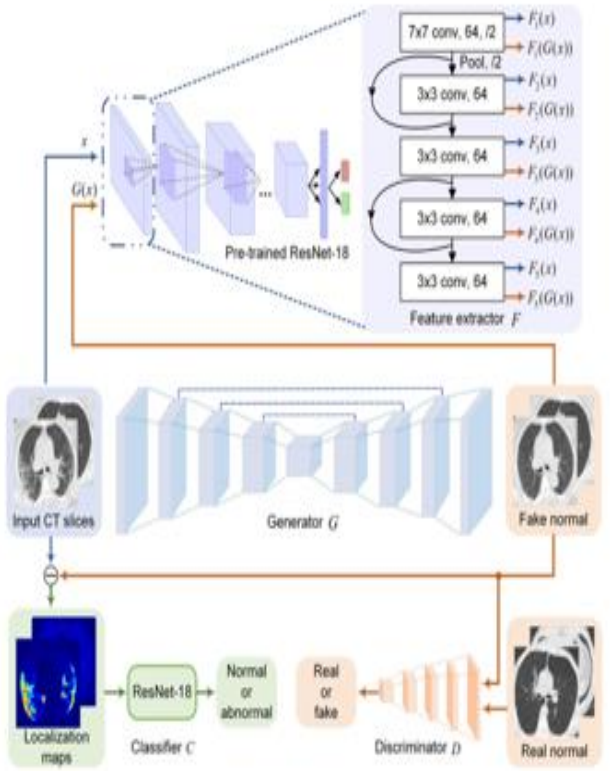

Fig 1: depicts the network architectureproposed for COVID-19 lesion localization. The patch discriminator and the encoder-decoder collaborate to eliminate probable COVID-19 lesions from input CT slices. To improve the image quality of the generated CT slices, shallow layers of the pre-trained ResNet-18 are used to perform low-level feature matching between inputand output. The localization maps are classified using another ResNet-18.

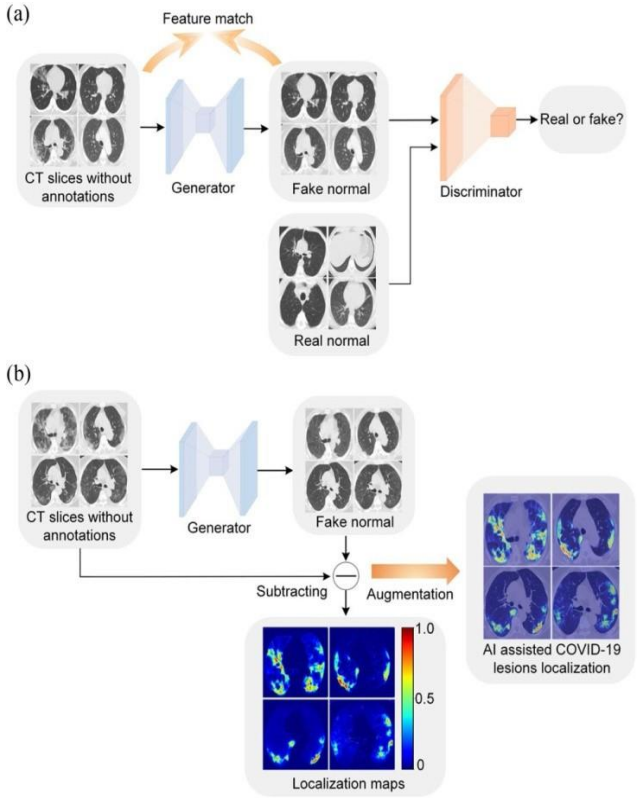

Fig 2: depicts an overview of the proposed COVID-19 lesion localization method. (a) A generator and a discriminator collaborate to eliminate possible lesions during model training. Feature matching improves the picture quality of the produced fake normal images. (b) During model inference, we derived the localization map by subtracting the generator's output from its input. The localization map is superimposed onthe original picture to help with the COVID-19 diagnosis.

COVID-19 lesion segmentation is another type. Fanetal., for example, provide an automatedCOVID-19 lung infection segmentation approach based on a carefully built network combined with edge information from infected areas and show that segmentation accuracy may be further enhanced by employing pseudo segmentationlabels.Wang et al. offer a noise-resistant architecture for COVID-19 lesion segmentation toaddress the erroneous annotation caused by pneumonia lesions' complicated appearances and substantial inter- and intra-observer variability. These supervised learning approaches appear to be more accurate than weakly supervised visual augmentation techniques in terms of automated segmentation of lung infected areas. However, in order to produce promising results, such fully supervised learning approaches need huge pixel- level annotated CT slices. Most available COVID-19 CT scan datasets with human labelling of diseased areas could not match this need. In contrast, the majority of existing COVID-19datasets just give patient-level labels (i.e., class labels) to indicate whether a person is infected or not, with no detailed annotations. To address the fore mentioned short com

We developed a weakly supervised learning strategy for accurate COVID-19 lesion localisation based on generative adversarial network combing with feature match, as seen in Fig. 1. A generator, a discriminator, and a feature extractor were included in the suggested model. By re-moving ground-glass opacity (GGO) andpulmonary consolidation from CT slices with COVID-19, the generator and discriminator collaborated to generate a normal-looking picture. The intricate texture of chest CT scans, on the other hand, may not be properly represented by such a GAN-based architecture. We created a feature extractor to instruct the generator to outputpictures with similar low-level characteristics to the inputs, which boosts lesion localization accuracy.We created a diagnostic system with better classification accuracy and interpretability by providing the GAN-based framework with a classifier branch. During the global SARS-CoV-2 outbreak, computer-aided diagnosis of COVID-19using chest CT is critical.We demonstrated in this study that the proposed method could relieve radiologists of laborious workloads, thereby contributing to the large-scale screening of COVID-19.

ISSN No:-2456-2165

II. BEHAVIORAL MAPPING AND TRACKING

Behavioural mapping is a research tool used to observe and record patterns in a particular setting at a particular time. Behavioural mapping can be either location-based or individual-based, depending on whether the focus of observation is to identify location wise behaviours or individual-based patterns o

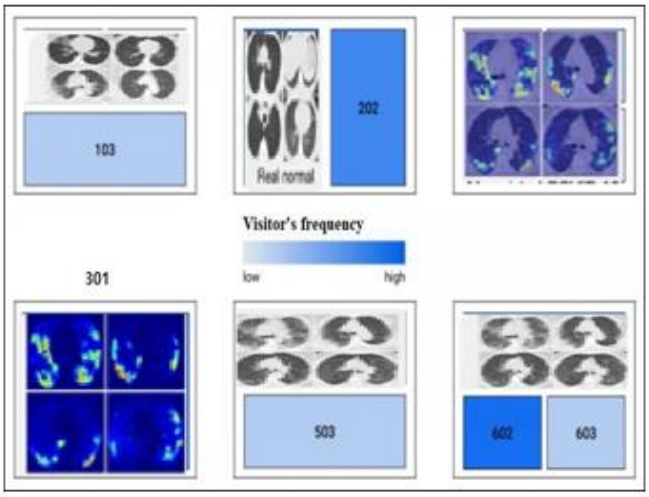

Fig 3- Behavioral Mapping and TrackingMETHODOLOGY

This work involved three datasets. The initial dataset came from Brazil and included 1252 CT scans that were positive for SARS-CoV-2 infection (COVID-19) and 1230 CT scans from patients who were not infected with SARS-CoV- 2, totaling 2482 CT images from 120 patients.These statistics were gathered from actual patients in hospitals in Sao Paulo, Brazil. However, there were no segmentation labels in this dataset, andwe simply utilised it for training. We gathered the second dataset, which comprises of 98 axial CT slices from various COVID-19 patients, to test the proposed method's lesion localization accuracy.The Italian Society of Medical and Interventional Radiology collected all of the CT slices. A radiologist used different labels to segment theCT pictures, detecting lung infections The 98 CT slices were separated into two groups: validation and testing. The validation set contained 50 CT slices with the goal of adjusting hyperparameters and selecting a model. The model's performance was evaluated using the remaining 48 CT slices. This testing set was designated as Testing Set1.The third study came from China Medical University and included 300 CT images from seven individuals infected with SARS-CoV-2. Because pixel-level annotations are not available in this dataset, we invite a radiologist to assess the accuracy of lesion localization. This testing set was designated as Testing Set 2.

➢ *Network Architecture*

When only image-level labels were provided, our objective was to reliably pinpoint possible lesions on CT slices using COVID-19. We suggested an unique weakly supervised learning approach based on this assumption, employing GAN with feature match. A generator with an encoder-decoder architecture was trained to remove potential COVID-19 features and generate bogus CT slices. The input CT slices included both normal and abnormal cases.

Unusual circumstances The generator was normal inthe input slices,was attempting to produce slicesthat were the same as inputs The infected COVID- 19 lung area may be easily located and segmented by subtracting the generator's output from the relevant inputs.

To assist the generator in producing a CT slice that seems to be genuine normal, a discriminator was included to determine if the output CT slice wasreal normal or fake normal. The discriminator assisted the generator in removing as many COVID-19 signals from the original CT slice as feasible. It is obvious that the generator and discriminator create a generative adversarialnetwork (GAN). It is crucial to highlight that paired photos are not required for model training,It has been demonstrated that CNN features retrieved from shallow layers respond to corners, edge/color conjunctions, and mesh patterns. The L1 loss of these matched characteristics was then calculated. The feature-level loss aids in the matching of low- level features between the generator's input and output, improving the realism of the generated pictures.

In addition, by incorporating a classifier branch into the network, we may create a diagnostic system based on localization maps. If the classifier's input only contains lesions for abnormalphotos and nothing for normal images (zero values everywhere), the classifier would be able to predict the category of the incoming images more quickly and precisely. Furthermore, building a more accurate classifier may aid the generator's output in retaining normal areas while eliminating lesions from the original picture.

➢ *Loss Function*

The goal was to develop a mapping function G: X -> Y between two domains X and Y using training examples$\{xi\}^N X$ and$\{yj\}^M Y$,, where X represents CT scans with COVID-19 and normal CT slices, and Y represents normal CT slices. To differentiate between slices y and translated slices G, a discriminator D is utilised (x). Our goal included four terms: adversarial losses for matching the distribution of generated images to the distribution of data in the target domain; a consistency loss to emphasise the similarity between the generator'soutput and input; a feature match loss to guide the generator to perform feature matching; and a cross-entropy loss to train the classifier. G: X ->Y and its mapping function where G attempts to produce pictures G(x) thatresemble images from the domain Y, while D attempts to discern between translated samples G(x) and genuine samples y. It was worth noticing that (1) differed from the original implementationof GAN. We replaced the negative log-likelihood goal with a least-square loss. This loss performs more consistently during training and produces higher-quality results. The consistency loss and feature match loss may be stated as

$$Lcons\ (G,X)=Ex\sim pdata(x)[|G(x)-x|1\ ]$$

$$Lfeat(G,\ F,\ X)\ =\ Ex\sim pdata(x^{\Sigma}\ \ w|F\ (G(x))\ -\ Fi(x)|1$$

ISSN No:-2456-2165

where 1 denotes the L1 norm, F is a feature extractor, and Fi(x) signifies the feature map computed by forwarding propagation after the ith convolutional layer of F under the input x as illustrated in Fig. 2, wi determines the relative priority of the five objectives. The cross-entropy loss may be calculated as follows:

$$L(G,C)=E[-t\log(s)-(1-t)\log(1-s)] \quad (4)$$

$$ce \qquad x\sim pdata(x)$$

$$s=C(\varphi(x-G(x))) \quad (5)$$

where C is a classifier, C(x) is the classifier's outputfor the input x, φ(x G(x)) is the localization map, t represents classification labels, normal cases are designated as 0, abnormal cases are marked as 1, and φ is a ReLU activation.

The total loss function for optimizing theproposed model was

$$Ltotal(G,D,C)=-Lgan(G,D,X,Y)+\alpha Lcons(G,X)+\beta Lfeat(G,F,X)+\gamma Lce(G,C) \quad (6)$$

where$\alpha,\beta,$and γ are three hyper- parameters for losses balancing.

We aimed to solve:

$$G^{*}=\text{argmin max } Ltotal(G,D,C) \quad (7) G,C \qquad D$$

It's worth noting that the feature extractor F was pre-trained in a binary classification task, so we didn't have to update it during GAN training.

➢ *Implementation Detail*

The PyTorch framework was used to run experiments on an NVIDIA GeForce GTX 1080TI with 11 GB RAM. The generator G was updated using the Adam optimizer with a learning rate of 5e-6. TTUR were employed to stabilise training by setting the discriminator D's learning rate to four times G. The classifier C was trained at a rate of 1e-4. Due to GPU memory limitations, we utilised a batch size of 8. During training, samples were horizontally and vertically flipped and scaled to 256 256 on the fly, and pixel values were normalised from 0 to 1 before being sent to the model.

As the generator G in our tests, we employed a modified U-Net. We specifically changed the max pooling operation with a 3X3 convolution with a stride of 2. In order to improve discrimination between different produced slices, batch normalisation was substituted by instancenormalisation. To prevent gradient vanishing, residual connections were added to each convolution block. As the discriminator D, a patch GAN was utilised, which produced a N N array rather than a single scalar output signalling true or false. To stabilise GAN training, a mini-batch standard deviation layer was added to the second tolast convolutional layer of Patch GAN. As the classifier C, we utilised a ResNet-18.

The training set contained 2482 CT scans with only image-level labels available. Real normal slices for training the discrim-inator were the 1230 normal CT slices from the trainings. The validation set includes 50 CT slices annotated at the pixel level. Our model was tested using two sets of data: Testing Set 1 (48 CT slices with pixel- level annotation) and Testing Set 2 (300 CT slices without labels). During model training, an alternate technique was used by iteratively updating differentportions of the model,

$$\max L1=-Lgan(G,D,X,Y)+\alpha Lcons(G,X) \quad (8) GD$$

$$\text{Min} L2=\beta Lfeat(G,F,X) \quad (9)$$

$$G$$

$$\min L3=\gamma Lce(G,C) \quad (10)$$

$$G,C$$

where α is set to 3.0, β is set to 1.0, γ is set to 0.4 as suggested, and hyper-parameters w1, w2, w3, w4, and w5 were set to 3.0, 2.5, 2.0, 1.5, and 1.0, respectively. Note that we treated the local, respectively. Note that we treated the localization map φ(x G(x))in (5) as a fixed constant while updating (10),This suggests that we did not change the generator G's settings when training the classifier C. This option was discussed in Section III.F. We employed a gaussian kernel withσ = 4.5 to smooth the findings because the localization map created by the suggested approach was scatter and mightinclude some noise. Finally, the localization mapwas mapped using min-max normalisation on a scaleof 0 to 1.

III. EXPERIMENTS AND RESULTS

➢ *Compare With Different Weakly Supervised Learning Methods.*

To assess the performance of the proposed weakly supervised learning method for COVID-19 infected region localization in CT slices, we compared it to three widely used weakly supervised object location methods, including Grad-CAM, Smooth-Grad, andmulti-scale Grad-CAM, which were recently applied to COVID-19 localization from CT slices. These three approaches were likewise trained using solely image-level labels from the training set. The obtained localization maps were normalised on ascale of 0 to 1.In Testing Set 1, all poorly supervised learning techniques were tested. The pixel-level area under the curve (AUC) scores of our proposed approach, multi-scale Grad-CAM, Grad-CAM, and Smooth-Grad were 0.883, 0.712, 0.674, and 0.530, respectively. Figure 3 depicts the matching receiver operating characteristic (ROC) curve (a). We discovered that the suggested technique could exactly pinpoint contaminated regions, whereas the other three methods could only approximately identify potentially infected regions.We also discovered that Smooth-Grad performs significantly worse than other poorly guided localization algorithms. Because pneumonia lesions frequently shared low-level features with surrounding tissue,using gradients with respect to the input images as a proxy for feature importance is not ideal. To further show the usefulness of the

ISSN No:-2456-2165

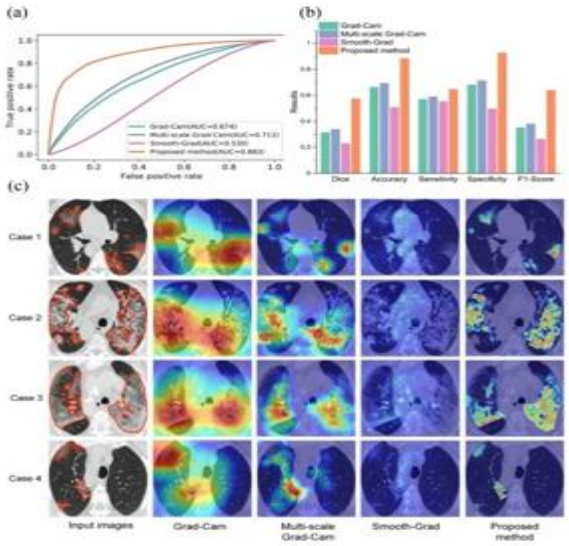

Fig 4: A comparison of several weakly supervisedlearning techniques in Testing Set 1. (a) The ROC curve for COVID-19 lesion localisation using severalpoorly supervised learning algorithms. (a) Quantitative evaluation of various poorly supervised learning techniques. (c) Qualitative comparison of several unsupervised learning approaches. In the input photos, lesions are represented by orange colour outlines.

Suggested technique, we turned the localization maps into binary pictures in the validation set using the grid search threshold. The Binary pictures indicate potentially contaminated areas. To analyse segmentation outcomes, we utilised dice coefficient, accuracy, sensitivity, specificity, and F1-score as performance measures. With a dice coefficient of 0.575, the suggested technique outperforms the otherthree ways by a wide margin, demonstrating the efficiency of our proposed method. Furthermore, we provide qualitative examples of numerous common lesion localization outcomes.

➢ *Compare With Fully Supervised Learning Methods*

In this set of studies, we tested the suggested approach's segmentation accuracy by comparing the segmentation results to the state-of-the-art segmentation method known as Inf-Net. Inf-Net was trained on a training set of 50 CT slices and tested onthe same 48 CT slices as us. We wanted to see if the weakly supervised learning

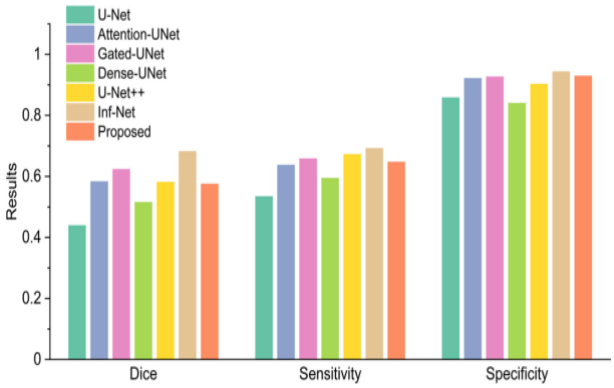

Fig 5 shows the comparison of fully supervised learning methods in Testing Set 1.

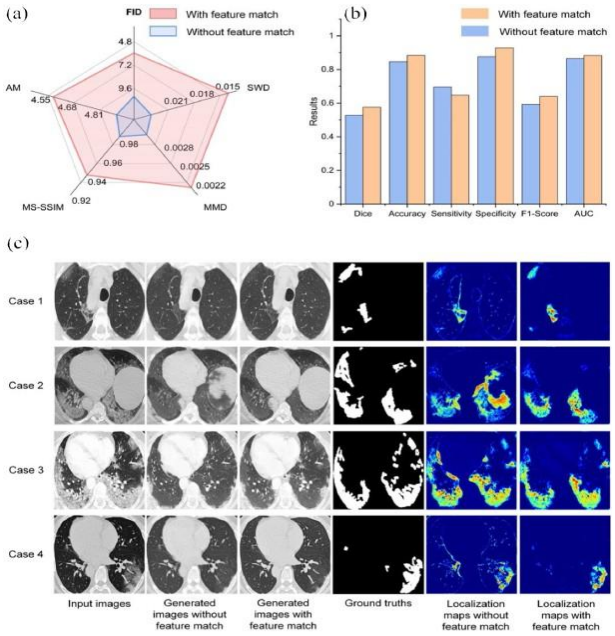

Fig 6: Feature match analysis in Testing Set 1.

(a) Comparing picture quality with and without feature matching. The lower the metric, the better.
(b) Lesion localization performance with and without feature match. (c) A qualitative evaluation of feature matching with and without.

Approach could be used instead of the fully supervised learning method because the annotateddata was restricted. To evaluate the segmentation outcomes, we employed dice coefficient, sensitivity, and specificity. compares the proposed weakly supervised learning approach to various fully supervised learning methods In all performance measures, the suggested technique outperformed U- Net and Dense U-Net trained in a fully supervised way,while **Inf-Net was superior.**

➢ *Feature Match Increases the Accuracy of Lesion Locali zation*

- *We explored the impact of feature match approachon infected region segmentation in this set of trials.*

As performance measures for image quality, we employed Fréchet Inception distance (FID), activation maximisation score (AM), maximum mean discrepancy (MMD), multi-scale structural similarity (MS-SSIM), and sliced Wasserstein distance (SWD). For quantitative assessment of lesion localisation, we employed the dice coefficient, sensitivity, specificity, F1-score, and AUC. As shown in Fig. 5(a), using feature match in the model improves picture quality and leads in more precise lesion location. However, wediscovered that adding feature matching to the model reduces sensitivity. This finding is most likely due to the fact that generated slices with less detailedinformation tend to produce over-segmented results, resulting in ahigher sensitivity.

ISSN No:-2456-2165

➢ *Visualization Comparison Between Different Methods*

The 300 COVID-19 CT slices in this investigationwere classified as mild, common, severe, and critical based on the severity by calculating the percentage of lesion to lung size, with mild: 10%; common: 10%; severe: 30%; 50%; and critical: more than 50%. The sample sizes for mild, common, severe, and critical were 77, 152, 50, and 21, respectively, and the proportion of lesion to lung size for each cohort was 5.46% ±2.41%, 20.32%±5.80%, 39.45%±6.00%, and 59.64%± 5.96%.

The association between severity and visual score was next examined, with the visual scores of moderate,common, severe, and critical being 3.77± 1.01, 4.78± 0.44,

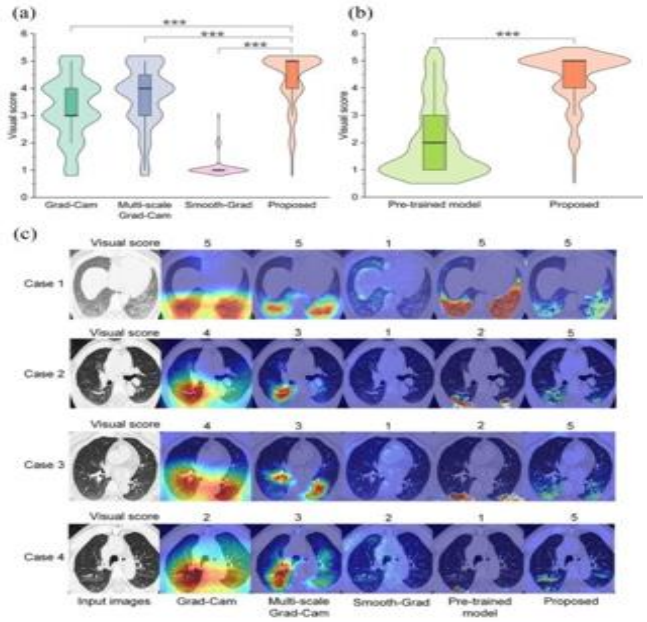

Fig 7: Visual score comparison acrossdifferent approaches in Testing Set 2. (a) Aquantitative comparison of multiple weakly supervised learning approaches was performed using a Student's t-test, with P values of $^{*}P<0.05;^{**}P<0.01;^{***}P<0.001$. (b) In comparison to a fully trained fully supervised learning model.(c) A qualitative comparison of several methodologies.

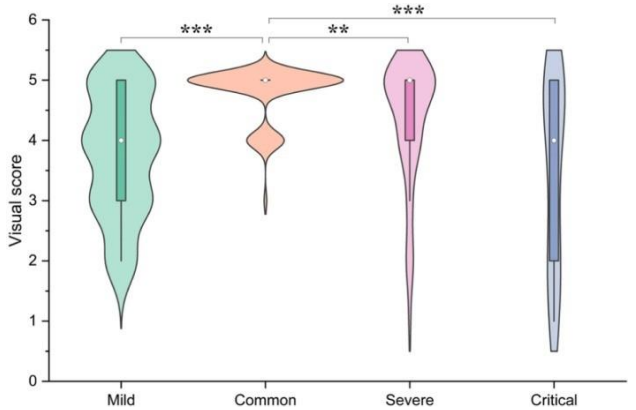

Fig. 8. Correlation between severity and visual score. The severity was divided into mild,common, severe and critical according tothe percentage of lesion to lung size (mild: percentage <10%, common:10% <percentage <30%, severe: 30%<percentage <50%and critical: percentage >50%). We comparedthe visual score between common group and the other groups with a Student's t-test,$^{*}P<0.05;^{**}P<0.01;^{***}P<0.001$.

4.32 ±1.04, and 3.48± 1.54, respectively. According to our findings, The common cohort had the highest sample number, and its visual score was greater than that of the other three cohorts, with statistical differences (P 0.05).

➢ *Evaluate the Classifier*

We explored the impact of the classifier branch on lesion localisation and evaluated classification accuracy in this set of tests. We wanted to discover ifthe classifier C might increase the accuracy of lesion localisation.

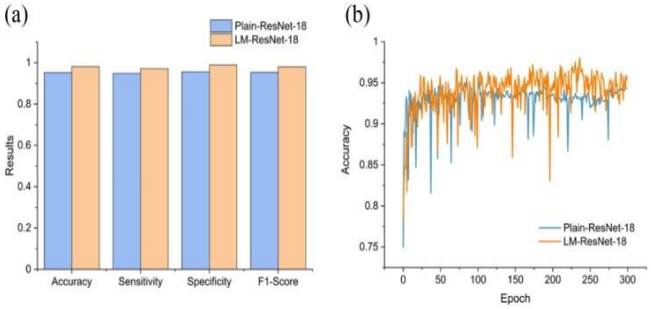

Fig 9 shows a comparison of Plain-ResNet-18 and LM-ResNet-18 categorization results. (a) Plain- ResNet-18 and LM-ResNet-18 classification performance. (b) Plain-ResNet-18 and LM-ResNet-18 testing curves.

As suggested, we set the hyper-parameter in (10) to 0.4. We compared the segmentation accuracy of updating generator G and classifier C simultaneously versus only updating classifier C. The outcomes are displayed. The classifier G might not benefit the generator G. As a result, during training the classifier, we set the localization map as a fixed constant.

Because Testing Sets 1 and 2 contain only positive samples, we randomly divided the 2482 CT slices with image-level labels (original training set) into a training set (n = 1737) and an independent testing set(n = 745) to assess classification accuracy. It should be noted that Testing Sets 1 and 2 were not included in this experiment. Because the classifier C's inputs were localization maps, we named it LM-ResNet-18. For comparison, we created a baseline model (ResNet-18) trained on original normal and pathological CT scans. Plain-ResNet-18 is the name we gave to the basic model. During experiments, the hyper-parameters of these two models stay constant. For a fair comparison, the data augmentationsoutlined in Section II.D were also used during training in Plain-ResNet-18. The classification results of Plain-ResNet-18 and LM-ResNet-18 areshown in Fig. 8(a). The accuracy, sensitivity, specificity, and F1-score of the LM-ResNet-18 were 0.982, 0.972, 0.989, and 0.981, respectively, whereas the Plain-ResNet-18 achieved 0.953, 0.949, 0.956,and 0.954. The testing curves for the two models are shown in Fig. 8(b). Because the localization maps are constantly updated during training, the LM-generalization ResNet-18's capacity may be increased.

ISSN No:-2456-2165

IV. DISCUSSION

We suggested an unique weakly supervised learning strategy for COVID-19 lesion localisation in this paper. Our technique outperformed other commonly used weakly supervised learning methods in terms ofperformance. This AI research was motivated by the aim to create a tool to help radiologists tackle the epidemic. The suggested solution can reduce radiologists' effort by providing COVID-19 cues in a visual augmentation mode. Furthermore, the generated localization maps can be used as pseudo labels, which radiologists can refine as annotations. This human-in-the-loop strategy can significantly reduce annotation time. Lung lesion localisation is critical in the COVID-19 diagnostic approach because it delivers explainable findings, whereas the CNNs-based classification model can only provide final judgments with no reasoning capability. Cam- based methods and gradient-based methods are proposed to provide a solution to the CNNs-based classification model's flaw, findings that may be explained to back up ultimate judgments.

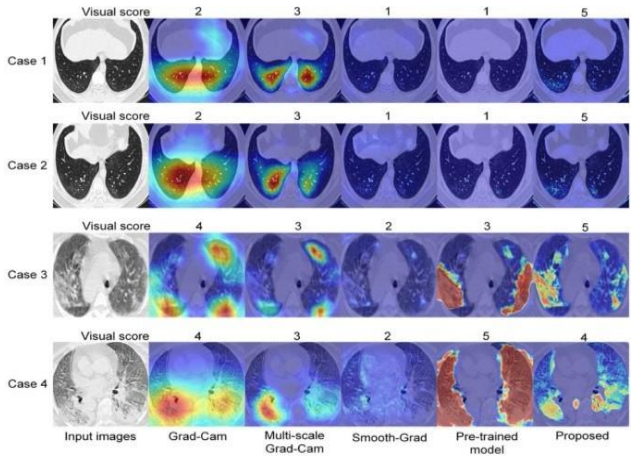

Fig 10. Qualitative assessment ofmodel robustness.

However, after training a classifier, these poorly supervised learning visualisation approaches can only estimate locate possible biomarkers in pictures at low resolution. We showed that the GAN-based weakly supervised learning system can reliablypinpoint COVID-19 lesions at high resolution. Aside from that, we discovered that multi-scale Grad-Cam outperforms single-scale Grad-Cam, implying that multi-scale characteristics aid in object localisation. This discovery also demonstrates the efficacy of the suggested technique in lesion localization since the generator attempts to combine characteristics fromall levels rather than manually selecting data from a specific level to construct the localization map.

Several research utilising fully supervised learning approaches have yielded encouraging results inCOVID-19 lesion segmentation. However, in orderto prevent over-fitting, these fully supervised learning algorithms need a massive scale of pixel- level annotations. We introduced another approach that performs well, is based on GAN with feature matching, and does not require pixel-level annotations in this paper. The suggested weakly supervised algorithm produces a competitive outcome with a dice coefficient of 0.575 when compared to fully supervised learning methods trained on 50 CT slices with pixel-level annotations. However, the dice coefficient of 0.575 is significantly lower than the fully supervisedtechnique trained on a large-scale dataset with pixel- level annotations.

A decent AI-assisted COVID-19 diagnosis toolshould provide visual signals to aid decision-making.To determine if the proposed technique provides radiologists with valuable visual information, we developed a metric called visual score that estimates the degree of overlap between the prediction localization map and the ground truth localizationmap. The suggested technique yielded encouraging results in Testing Set 2 with a visual score of 4.35±0.96, suggesting that the prediction findings are highly compatible with the observations and may be used to support the radiologist's final choice. We alsosee that the pre-trained fully supervised model performs worse than the suggested technique, as shown in Fig. 6. (b). This conclusion is most likely owing to the domain difference between their training set and our Testing Set 2, as well as the Image pre-processing differs between their approach and ours. This discovery also highlights theAI system's existing flaws, as these systems are fragile and sensitive to minor changes in data distribution [47]. Retraining the model on a new dataset is one solution to this problem. In this scenario, weakly supervised learning approaches have a significant benefit since we just need to supply weak labels for the new dataset rather than comprehensive annotations as in fully supervised learning.

We also looked at the relationship between severity and visual score to see how accurate our diagnostic augmentation technique was in COVID-19 patients with varying degrees of pulmonary lesion severity. We discovered that the lesion localization findings inthe common severity cohort with the highest visual score were very consistent with the radiologist (Fig. 7). Meanwhile, the common cohort accounted formore than half of the research cases (152/300), which is greater than the other three cohorts combined. These findings imply that the suggested technique may be used to quickly screen individuals with common severity, as measured by the proportion of the damage to the body.

lung size, which can aid in the fast identification of COVID-19 during major outbreaks and epidemics, particularly in large populations with shared severity. The visual scores for the mild and critical cohorts were 3.77 ±1.01 and 3.48 ±1.54, respectively, which were likewise satisfactory and proved the robustness of the suggested technique. Some extreme instances' qualitative outcomes We can tell from the radiologist's visual evaluations that the suggested technique is more resilient than existing ways. Furthermore, we can see from the first two instances in Fig. 9 that the suggested technique may aid radiologists in recognising some lesions that are difficult to detect.

Several research have also suggested using the GAN-based framework for lesion localisation. However, due to the complex texture of chest CT images, these GAN-based frameworks are not adequate for COVID-19 lesion localization. Based on this discovery, we presented a feature

ISSN No:-2456-2165

match technique toaid the model in capturing the complex texture of chest CT images, hence improving image quality. We discovered that feature matching might help the model create photos with finer-grained textures by reducing noise. We demonstrated that combining the GAN-based framework with feature matching improves lesion localization accuracy. Overall, the feature match strategy was a straightforward but effective way to improve the GAN-based framework for lesion localization.

We may further construct a diagnostic system with strong interpretability by adding a classifier branchto the network [17], because the diagnosis findings are based on infected areas. The diagnosis system may not only offer diagnosis findings but also the location of the lesion. As demonstrated in Fig. 8, the diagnostic system outperformed the vanilla classifier trained on original CT slices in classification performance. The shown lesion localization and classification accuracy showed that the proposed GAN-based diagnosis system might be used in place of the CAM-based diagnosis system. This diagnostic augmentation technique relieves part of the burden on clinicians by minimising reliance on personal experience and labor-intensive practise andconfirmation. Doctors may make faster and more accurate judgements using the proposed enhanced lesion diagnosis technology, while non-professionals,such as medical interns and general practitioners, can do pseudo-professional diagnoses.

The following are the limitations of our investigation. First, the suggested technique can only offer probable lesion localisation without distinguishing between GGO and pulmonary consolidation, which is very important in determining severity.

Second, because this study's analysis is based on slice-level data rather of volume-level data, the study's findings cannot be applied to volume-level situations. However, by aggregating the findings inside a CT volume, the suggested technique may simply be expanded to volume-level applications.

Behavioural mapping is a research tool used to observe and record behaviours in a particular setting at a particular time. Behavioural mapping can be either place-based or individual-based, depending on whether the focus of observation is to identify locational wise behaviours or individual time-based patterns of behaviours.

This is an example of how observation can be used to visualize how many visitors visited various booths at a exhibition fair. The map shows the frequency of visitors and reveals the booths most heavily and least heavily visited. Insights can be used to improve fair service, and attracting more visitors.

V. CONCLUSION

Feature match weakly supervised learning approach for COVID-19 lesion localisation. The generator is used to convert a CT slice with lesions into the matching slice with the lesions eliminated, while the discriminator is used to enhance the generator to produce more realistic-looking fake normal CTslices. A pre-trained feature extractor is utilised to enrich the fine-grained features in order to improve the picture quality of the produced slices. To stabilise model training, many techniques such as improved loss function, TTUR, and mini-batch standard deviation layer are applied. The experimental results confirmed the proposed method's superiority, which significantly outperformed other widely used weakly supervised localization methods. Furthermore, the proposed method yields a competitive result,In the lesion segmentation task, the fully supervised method outperformed the unsupervised method. We believe that the proposed method can be used as a powerful tool to alleviate the expert annotation cost bottleneck and advance the progress of computer-aided COVID-19 diagnosis.

REFERENCES

[1] C. Wang, P. W. Horby, F. G. Hayden, and G. F. Gao, “A novel coron-avirus outbreak of global health concern,” Lancet, vol. 395, no. 10223,pp.470–473,2020.
[2] C. Huang et al., “Clinical features of patients infected with 2019 novelcoronavirusinWuhan,China,”Lancet, vol.395,no.10223,pp.497–506,2020.
[3] Y. Fang et al., “Sensitivity of chest CT for COVID-19: Comparison toRT-PCR,”Radiology,2020,Art.no.200432.
[4] T. Aietal., “Correlation of chestC Tand RT-PCRtestingincoronavirusdisease 2019 (COVID-19) in China: A report of 1014 cases,” Radiology,2020,Art. no.200642.
[5] D. S. W. Ting, L. Carin, V. Dzau, and T. Y. Wong, “Digital technology andCOVID-19,”NatureMed.,vol.26,no.4,pp.459–461,2 020.
[6] H. X. Bai et al., “AI augmentation of radiologist performance in dis-tinguishing COVID-19 from pneumonia of other etiology on chest CT,”Radiology,2020,Art.no.201491,doi:10 .1148/radiol.2020201491.
[7] M. Tan and Q. V. Le, “EfficientNet: Rethinking model scaling for convo- lutional neural networks,”2019.[Online].Available: http://arxiv.org/abs/1905.11946
[8] X. Wang et al., “A Weakly-supervised framework for COVID-19 classi- ficationandlesionlocalization fromchestCT, ”IEEETrans.Med.Imag., vol.39,no.8, pp.261 5–2625,Aug.2020. This research provides a GAN combining with
[9] R.R.Selvaraju, M.Cogswell, A.Das, R.Vedanta m,D. Parikh, and D.Batra, “Grad- CAM: Visual explanations from deepnetwork sviagradient- based localization,”inProc.IEEEInt.Conf.C omput.Vis.,2017,pp.618–626.

[10] S. A. Harmon et al., "Artificial intelligence for the detection of COVID-19pneumonia on chest CT using multinational datasets," Nature Commun.,vol.11,no.1,pp.1–7,2020.
[11] H. Greenspan, R. S. J. Estépar, W. J. Niessen, E. Siegel, and M. Nielsen,"Position paper on COVID-19 imaging and AI: From the clinical needsand technological challenge stoinitial AIs olutionsatthe laband nationall eveltowardsane weraforAIinhealthcare,"Med.ImageAnal.,vol .66,2020,Art.no.101800.
[12] C.Jinetal.,"Developmentand evaluation of anar tificialintell igencesys- temfor COVID-19diagnosis,"NatureCommun.,vol.11,no.1,p p.1–14,2020.
[13] K.Gaoetal.,"Dual- branch combinati on network (DCN):Towardsaccu- rate diagnosis and lesion segmentation of COVID-19 using CT images,"Med.ImageAnal.,vol.67,2020,Art.n o.101836.
[14] L.Zhouetal.,"Arapid, accurateand machine- agnosticseg mentation and quantification method for CT-based COVID-19 diagnosis," IEEE Trans.Med.Imag.,vol.39,no.8,pp.2638–2652, Aug.2020.
[15] D.-P. Fan et al., "Inf-Net: Automatic COVID-19 lung infection seg- mentation from CT images,"IEEETrans. Med.I mag.,vol.39,no.8,pp.2626–2637,Aug.2020,d oi:10.1109/tmi.2020.2996645.
[16] G.Wangetal.,"ANoise- robustframework for automatic segmentation of CO VID-19 pneumonia lesions from CT images," IEEE Trans. Med. Imag.,vol.39,no.8,pp.2653–2663,Aug.2020.
[17] R.Zhangetal.,"Biomarkerlocalization bycomb ining CNN classifier and generativeadversarial network, "inProc.Int.Conf. Med.Image Comput. Comput.-Assist.Intervention,2019,pp.209–217.
[18] L. Sun,J. Wang, Y.Huang, X.Ding,H. Greenspa n,andJ. Paisley, "An adversarial learning approach to medical image synthesis for lesiondetection, "IEEEJ.Biomed. Heal. Inform .,vol.24,no.8,pp.2303–2314,Aug.2020.
[19] T. Xia, A. Chartsias, and S. A. Tsaftaris, "Pseudo-healthy synthesis withpathology disentanglement and adversarial learning," Med. Image Anal.,vol.64,2020,Art.no.101719.
[20] E.Soares, P. Angelov, S.Biaso, M.H.Froes, and D.K. Abe, "SARS-CoV-2CT- scandataset: Alargedataset ofrealpatients CTsc ansforSARS-CoV-2identification," medRxiv, 2020. [Online]. Available: https://www.medrxiv.org/content/10.1101/2 020.04.24.20078584v3
[21] "COVID- 19 CT segmentation dataset," https://medicalsegme ntation.com/covid19/,2020
[22] I.J.Goodfellowetal., "Generative adversarialn ets,"Adv. Neu-ralInf.Process.Syst., vol.3,pp. 2672–2680,Jan.2014,doi:10.3156/jsoft.29.5_ 177_2.
[23] K. He, X. Zhang, S. Ren, and J. Sun, "Deep residual learning for imagerecognition," in Proc. IEEE Conf. Comput. Vis. Pattern Recognit., 2016,pp.770–778.
[24] M.D. Zeilerand R. Fergus,"Visualizingandund erstanding convolutionalnet works, "inProc.E ur.Conf. Comput.Vis.,2014,pp.818–833.
[25] X. Mao, Q. Li, H. Xie, R. Y. K. Lau, and Z. Wang, "Multi-class gen-erativeadversarialnetworkswiththeL2lossfun ction,"2016,vol.5,pp.1057–7149,arXiv:1611 .04076.
[26] A. Paszke et al., "PyTorch: An imperative style, high-performance deeplearning library,"Adv. NeuralInf. Process. Syst., vol.32,pp.8026–8037,2019.